

# ADAPTIVE GROUND CLUTTER REMOVAL FOR TRIPLE-PRT SETUP

J. Sierwald\* and J. Huhtamäki†

Eigenor Corporation, Helsinki/Sodankylä, Finland

## 1. INTRODUCTION

The use of non-uniform pulsing intervals presents a solution to the so-called Doppler dilemma which restricts the measurement of high-speed targets with a pulsed Doppler radar at large distances (Pirttilä et al. (2005)). Contrary to popular belief that development of proper ground clutter removal algorithms for non-uniform sampling is impracticable, we demonstrate a ground clutter removal system with superior performance compared to standard schemes. The clutter removal algorithm utilizes dual-polarization information in detecting if a signal should be filtered, c.f. CMD by Hubbert et al. (2009).

Standard pulsing schemes, such as using uniform pulsing (single-PRT) or fast switching between two pulsing frequencies (dual-PRF), have their own advantages. These include, for example, simple and computationally inexpensive signal processing algorithms. Rapid development of modern processors has, however, relaxed the computational efficiency requirements for real-time analysis of a weather radar data. The adaptive clutter removal algorithm presented here is an example of a computationally more challenging method which is capable of operating in real time on an off-the-shelf personal computer through efficient utilization of the CPU's vector processor.

For the non-uniform pulsing scheme, we choose a triple-PRT setup capable of handling velocities up to 50 m/s with an operating radius of 260 km. In addition to the extended unambiguous velocity domain covering typical weather phenomena, advantages of using triple-PRT pulsing include improved reflectivity  $Z$  estimates from signals containing a ground clutter component. Moreover, due to the higher maximum velocity limit it is possible to obtain improved velocity distribution information through spectral analy-

sis. Standard dual-polarization products are estimated similarly as with other pulsing schemes.

The triple-PRT scheme is tested using a C-band weather radar during the spring and summer of 2012 in Helsinki, Finland. In the measurements, triple-PRT, single-PRT and dual-PRF schemes were operated consecutively separated by time intervals of a few minutes enabling direct comparison. The single-PRT and dual-PRF measurements were processed using the standard algorithms of Vaisala's RVP900 signal processor. In addition to measurements, the triple-PRT algorithm has been tested extensively using simulated data.

## 2. METHOD

### 2.1. Triple-PRT

In the triple-PRT scheme, patterns consisting of three pulses are sent repeatedly. The three pulses are separated by unequal time intervals, for example by 1750  $\mu\text{s}$ , 2000  $\mu\text{s}$  and 2500  $\mu\text{s}$ . Figure 1 illustrates the single-, dual- and triple-PRT pulsing schemes.

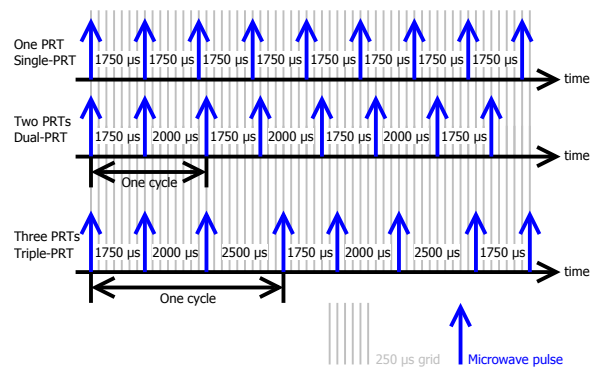


Figure 1: Illustration of single-, dual- and triple-PRT pulsing schemes.

\*Diesterwegstraße 3, 24113 Kiel, Germany, email: sierwald@eigenor.com

†email: jukka.huhtamaki@eigenor.com

The unambiguous velocity range for the different schemes is determined in theory by the greatest common divisor (GCD) of the pulse intervals. For example, for dual- and triple-PRT in this example, the GCD is 250  $\mu$ s, translating to a maximal unambiguous velocity of over 50 m/s for a C-band radar with  $\lambda = 0.0535$  cm. However, the time interval ratios must be chosen carefully for two reasons: the system must (1) be fault-tolerant against errors due to low signal-to-noise ratios (SNR) and (2) survive ground clutter filtering for various different input signals. Most importantly, we require that the reflectivity  $Z$ , velocity  $v$  and its Gaussian distribution width  $\sigma$ , can be estimated with high precision.

As described below in Subsection 2.3, the velocity and width estimation is based on comparing the auto-correlation function (ACF) of the input signal to a host of model ACFs. Figure 2 illustrates how easy it is to confuse two different ACFs within the unambiguous velocity domain using different triple-PRT ratios ( $\sigma = 1.0$  m/s). In the figure, the longest time interval is always scaled to 10, so that for example a ratio of (12:14:15) should be read as (8:9.3:10) where the first and second numbers are to be read as the x- and y-coordinates in the graph\*. In blue regions, there are at least two very similar model ACFs whereas in the dark red regions all the ACFs differ significantly. Therefore, by choosing a triple-PRT ratio of, say (7:8:10), it is much less likely to make an erroneous velocity estimation than with a ratio of (7:8.5:10).

Ground clutter removal causes two different complications in estimating the standard meteorological quantities. Depending on the signal velocity and width, the clutter removal process tends to reduce the observed reflectivity. The other consequence is that clutter filtering often distorts the calculated ACF, thus affecting the ACF comparison. Both effects can be reduced by sensible choice of the triple-PRT ratio.

## 2.2. Ground Clutter Removal

The high-pass FIR filter used in removing ground clutter is designed based on theory of statistical inversion. It can be shown\* that the optimal ma-

\*Loosely speaking, the diagonal in Fig. 2 can be considered as the dual-PRT scheme.

\*For more details on this, see a book titled *Triple-PRT Signal Processing for Weather Radars* by the authors (currently unpublished).

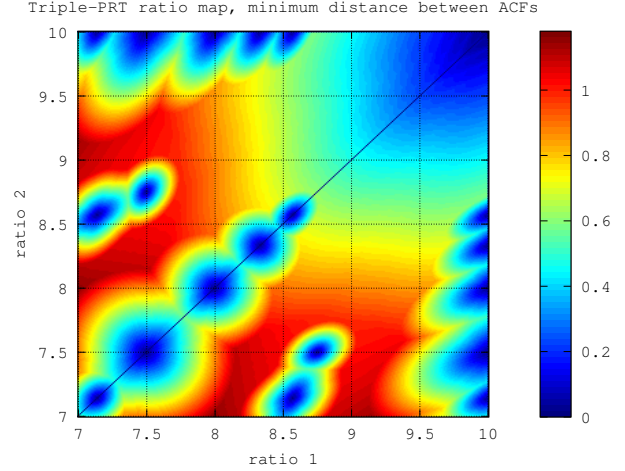


Figure 2: Minimal distance between ACFs for different triple-PRT ratios with  $\sigma = 1.0$  m/s and  $v \in [-50, +50]$  m/s.

trix for filtering a signal with a known ACF from an input signal is given by

$$G = \left( I + \frac{R_{gc}}{P_n} \right)^{-1}, \quad (1)$$

where  $R_{gc}$  is the covariance matrix of the signal to be filtered (ground clutter in this case) and  $P_n$  is the noise power. This filter matrix is similar to the one used in the GMAT algorithm (Nguyen et al. (2008)) with the relation  $G = (G_{GMAT})^2$ . A Gaussian model for ground clutter is used in constructing  $R_{gc}$ . A benefit of this technique is that it works for an arbitrary pulsing scheme.

Due to the destructive nature of clutter removal, we have devised an adaptive method of applying the clutter filter. For computational efficiency, a data sector of 8 degrees in azimuthal angle is processed at once. Figure 3 illustrates the steps taken in adaptive filtering. Data is processed using filters corresponding to several different strengths of ground clutter (controlled by the parameter  $P_n$  in Eq. (1)). Based on dual-polarization analysis and 2D textures, a filtered signal is chosen which relates to characteristics of precipitation the best. After choosing the best filtered candidate for all range bins, meteorological quantities are estimated from the filtered data.

The adaptive algorithm bases the decision if ground clutter should be removed on the following items:

- Value of  $ACF(T_{\text{pattern}})$ , where  $T_{\text{pattern}}$  is the total time interval of three consecutive pulses

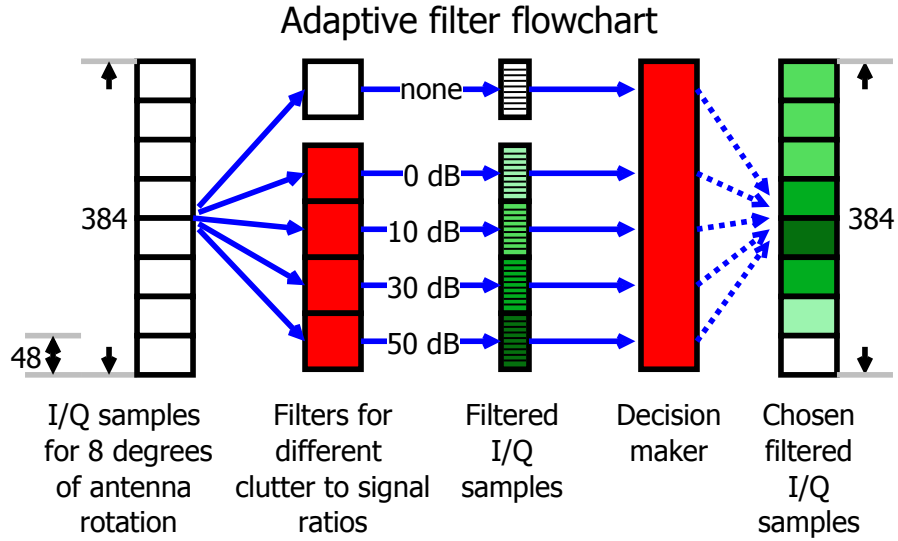


Figure 3: The ground clutter removal algorithm processes a chunk of data 8 degrees wide in the azimuthal angle. In this example, this translates to 384 time series samples for each range gate. Ground clutter filters of different strengths are applied to each input signal. Filtered signals which correspond the best to the nature of precipitation signals are chosen for further analysis.

(6250  $\mu$ s used in the measurements). Values are near  $1.0+0.0j$  if the velocity and width are near zero.

- Variability of the copolar differential phase  $\Psi_{dp}$  over range. A very good indicator for rain or snow. Less reliable for insects or inside the melting layer.
- Power variability over range and azimuth.
- Power loss due to filtering.
- Linear regression analysis of  $\Psi_{dp}$  using filtered data. The algorithm will compare the value of  $\Psi_{dp}$  to an expected value in rain.
- Receiver saturation check.
- Value of the copolar correlation coefficient  $\rho_{co}$  and its change in filtering.
- Result of the decision algorithm for neighboring gates.

Parameters used in the decision making are tuned to work well for rain and snow. Inside the melting layer the decision can err towards ground clutter removal, which may also happen with signals from birds. The decision making

must also consider the SNR, as the parameters become less reliable for noisy signals. If the input signal has a low SNR, results from the filters for a high clutter-to-signal ratio (CSR) do not have to be taken into account.

### 2.3. Velocity and Width Estimation

The method used for estimating velocity  $v$  and the width of its distribution  $\sigma$  relies on comparing the ACF calculated from the input time series data to a set of Gaussian model functions. The ACF of a precipitation signal with a Gaussian power spectral density has the form (Bringi and Chandrasekar (2001))

$$R(\tau) = P_p \exp\left(-j\frac{4\pi v_0}{\lambda}\tau - \frac{8\pi^2\sigma^2}{\lambda^2}\tau^2\right), \quad (2)$$

where  $P_p$  is the signal power,  $v_0$  and  $\sigma$  are the expectation value and standard deviation of the velocity  $v$ , and  $\lambda = 0.0535$  m is the wave length of the radar. The difference of the time series signal ACF and a model ACF is calculated with model parameters ranging from  $v \in [-50, +50]$  m/s and  $\sigma \in [0, 5]$  m/s. The estimated products  $v_{est}$  and  $\sigma_{est}$  are chosen by minimizing the distance to the

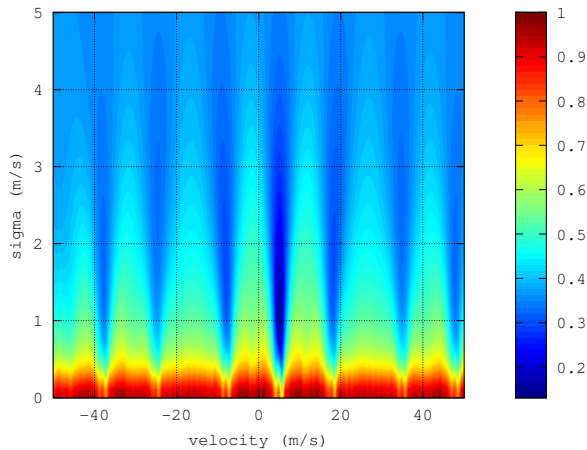


Figure 4: Difference of ACFs calculated for a simulated precipitation signal and a table of Gaussian model signals. The estimated velocity and width are evaluated by minimizing the difference (dark blue region).

model ACF table. Figure 4 illustrates the distance of a simulated signal with  $v_{\text{est}} = 5.0 \text{ m/s}$  and  $\sigma_{\text{est}} = 1.1 \text{ m/s}$  to the table of model functions.

If ground clutter is removed from the signal, the power is corrected based on  $v_{\text{est}}$  and  $\sigma_{\text{est}}$ . This correction factor can be evaluated by calculating the amount of power lost from applying the ground clutter filter to the Gaussian model precipitation signal (or directly to its ACF).

### 3. SIMULATIONS

We have tested our triple-PRT algorithm by analyzing simulated signals using both single- and dual-polarization simulators. In a typical simulation round a number of signal samples ranging from 5000 to 30000 are generated for each (expectation value of) velocity and width chosen. Accuracy of the estimation algorithm is tested by varying the SNR as well as the CSR.

In the absence of clutter or noise, the width and velocity are estimated precisely. The velocity bias in this case is illustrated by the green curve in Fig. 5 with  $\langle \sigma \rangle = 1.0 \text{ m/s}$ . The simulations reveal that even without a clutter component, application of the ground clutter filter degrades the performance of the velocity estimation by an order of 10 cm/s, as shown by the red line in Fig. 5. If ground

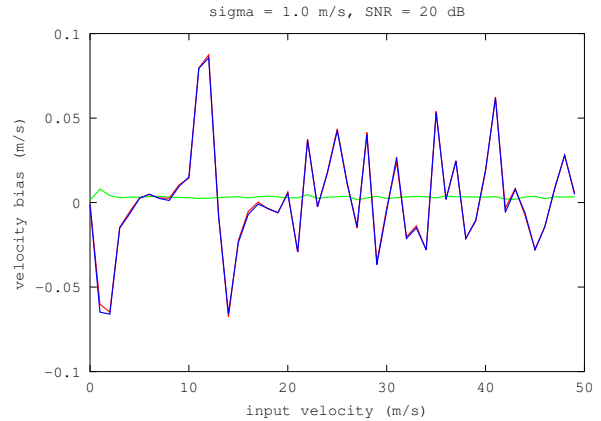


Figure 5: Bias of estimated velocity (y-axis) with 5000 simulated signals for each input velocity (x-axis): no clutter, no filtering (green), no clutter, with filtering (blue), and CSR=40 dB, with filtering (red). Application of the filter increases the bias, but addition of a clutter component does not degrade the performance further.

clutter is added, however, the performance of the method remains intact, as shown by the blue line in Fig. 5. This is one strong reason for adaptive application of the ground clutter filter.

In the case of noisy signals, e.g. SNR=0 dB, it often happens that the wrong local minimum in the ACF difference function turns out to be the global minimum leading to incorrect velocity and width estimation. We have calculated the resulting error rate ( $N_{\text{wrong}}/N_{\text{total}}$ ) using simulations. Figure 6 displays the calculated error rate as a function of input velocity for four different range integration lengths. The general conclusion is that some (pulsing-scheme dependent) input velocities are more difficult to estimate than others. For triple-PRT scheme used in the measurements (7:8:10), the error rate peaks at around 0 m/s, 13 m/s, 30 m/s and 43 m/s. If a longer range integration length is used, the estimation performance improves greatly. Also, using such method we have shown that ill-advised triple-PRT ratios, such as 7:8:9, often perform significantly less reliably than a carefully chosen ratio, see Subsection 2.1.

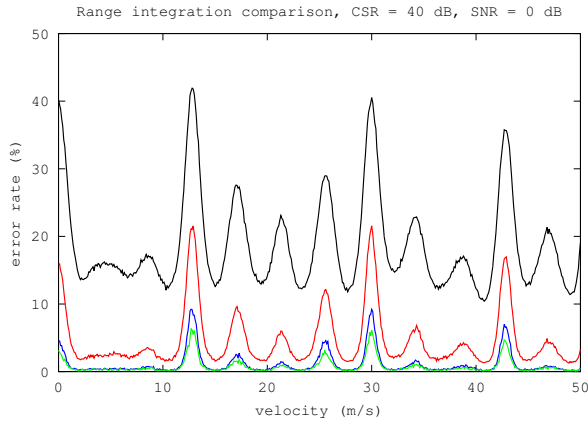


Figure 6: Error rates as a function of input velocity for four different range integration lengths: 150 m or no range integration (black), 300 m (red), 600 m (blue) and 900 m (green). In this simulation  $\langle \sigma \rangle = 1.0 \text{ m/s}$ ,  $\text{SNR}=0 \text{ dB}$  and  $\text{CSR}=40 \text{ dB}$ .

## 4. MEASUREMENTS

In order to test the triple-PRT scheme, we have carried out measurements which enable direct comparison of the method to standard pulsing schemes, namely single-PRT and dual-PRF. The measurements were made using the C-band dual-polarization radar located in Kumpula Campus at the University of Helsinki during spring and summer of 2012. The most distinctive advantage of triple-PRT and dual-PRF is, of course, the ability to measure higher wind velocities. The benefit obtained from the adaptive ground clutter filtering used in the triple-PRT measurements is most vividly visible in the disappearance of the so-called Doppler snakes, i.e. reflectivity valleys located at multiples of the Doppler folding velocity.

The weather events recorded include cases of strong winds, snowfall, rainfall, low-altitude melting layers and temperature inversion. In addition, we have analyzed data of anomalous propagation as well as signals from biological scatterers and various man-made structures. The measurements were run at 20 minute intervals resulting in several terabytes of stored I/Q data. A comprehensive discussion of the results will be published in a book. As an illustration, Fig. 7 shows a PPI plot comparison of a heavy rainstorm with wind speeds reaching over 30 m/s scanned in June 2012 in Helsinki. The triple-PRT setup uses the adaptive ground clutter removal discussed

in Subsection 2.2, the single-PRT employs the GMAP algorithm (Siggia and Passarelli (2004)) and the dual-PRF uses notch filtering (Sirmans (1992)).

## 5. CONCLUSIONS

By comparing the measurement results obtained using triple-PRT pulsing with standard pulsing schemes, we have concluded that the triple-PRT setup yields superior reflectivity and velocity estimates. The non-uniform pulsing extends the unambiguous velocity domain to cover typically encountered wind speeds of up to 50 m/s without constraining the estimation of other meteorological products. The limiting factors for ground clutter removal are the phase noise generated by the radar hardware and receiver saturation effects. The triple-PRT signal processing is able to remove at most 55 dB of power in the Kumpula Radar, which is consistent with the standard error of the phase of 0.1 degrees.

Clutter filtering is turned on only when needed improving reflectivity estimates by avoiding unnecessary weakening of the received signal, which usually takes place most prominently at the zero isodop (so-called Doppler snakes). Velocity and Gaussian width estimation, which is performed by comparing the ACF of the input signal to a host of model ACFs, appears to give reliable estimates even for low signal-to-noise ratios. This has been tested using both simulations as well as real-weather measurements. A method for correcting the reflectivity after ground clutter removal based on the estimated velocity and its Gaussian width, similar to the one employed e.g. in GMAP, is designed. Dual-polarization quantities can be estimated analogously independent of the pulsing scheme employed. Moreover, a method for choosing a good ratio for the triple-PRT timings is developed, minimizing the error rates observed in estimating meteorological quantities of interest.

Triple-PRT measurements employing pulsing schemes described in this document are currently ongoing at the Kumpula Radar. Further analysis will concentrate on using different pulsing intervals, RHI scans, the wide dynamic range setup as well as various weather events.

**Acknowledgement** This project was sponsored by the Finnish Funding Agency for Technology and Innovation TEKES as part of the MMEA program managed by CLEEN Ltd. For fruitful collaboration, we would like to acknowledge the Finnish Meteorological Institute, the University of Helsinki and Vaisala Group.

## References

Bringi, V. N. and V. Chandrasekar, 2001: *Polarimetric Doppler Weather Radar*. Cambridge University Press.

Hubbert, J. C., M. Dixon, and S. M. Ellis, 2009: Weather radar ground clutter. Part II: Real-time identification and filtering. *Journal of Atmospheric and Oceanic Technology*, **26**, 1181–1197.

Nguyen, C. M., V. Chandrasekar, and D. N. Moiseev, 2008: Gaussian model adaptive time domain filter (GMAT) for weather radars. *Geoscience and Remote Sensing Symposium*, **2**, II-509–II-512.

Pirttilä, J., M. S. Lehtinen, A. Huuskonen, and M. Markkanen, 2005: A proposed solution to the rangedoppler dilemma of weather radar measurements by using the SMPRF codes, practical results, and a comparison with operational measurements. *Journal of Applied Meteorology*, 1375–1390.

Siggia, A. D. and R. E. Passarelli, 2004: Gaussian model adaptive processing (GMAP) for improved ground clutter cancellation and moment calculation. *ERAD 2004 proceedings*.

Sirmans, D., 1992: Clutter filtering in the WSR-88D. *NWS/OSF Internal Reports*.

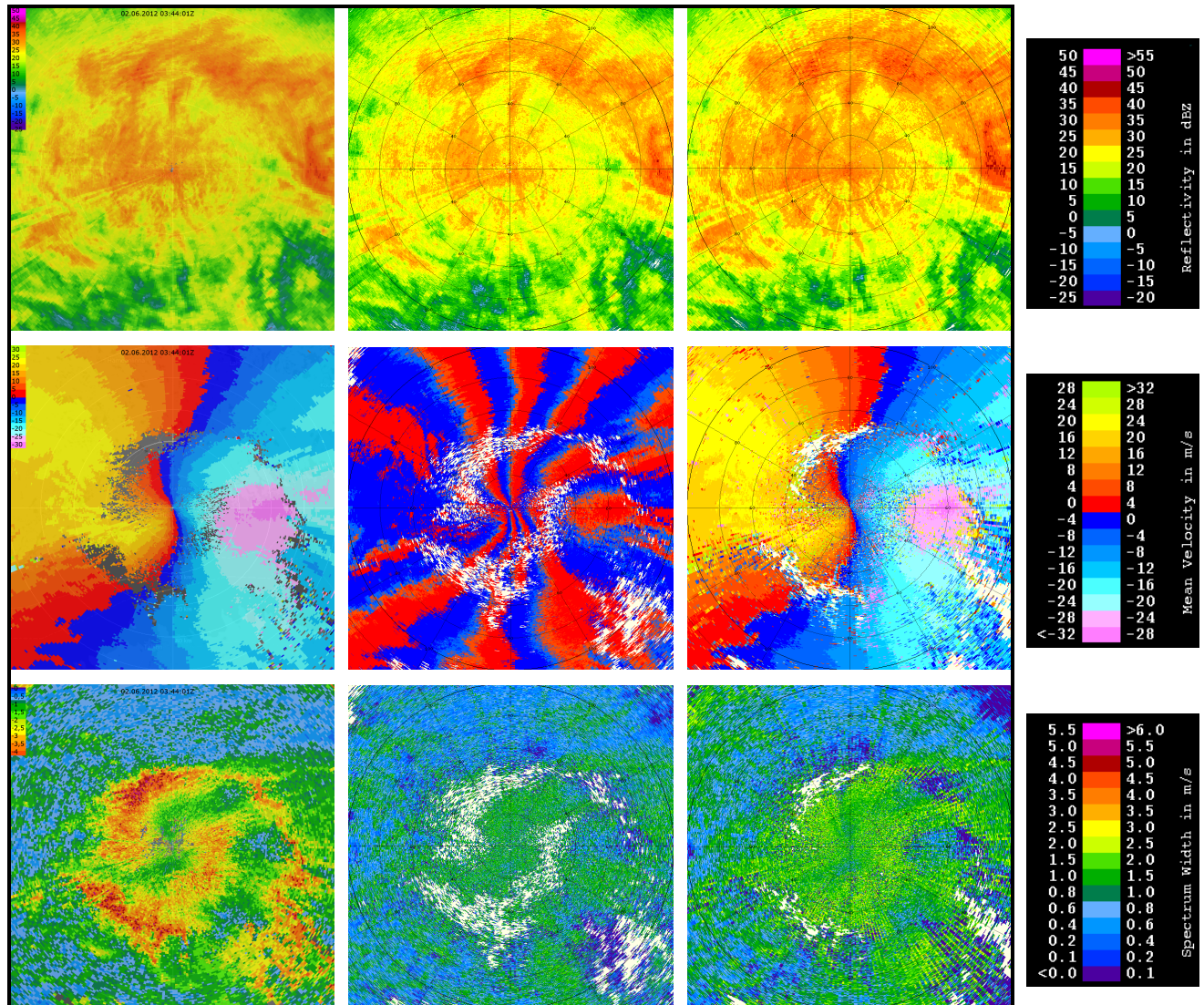


Figure 7: Scan of a rainstorm in Helsinki, June 2012, using an elevation angle of 0.5 degrees. The reflectivity  $Z$  (top), velocity  $v$  (middle) and width  $\sigma$  (bottom) are displayed for the triple-PRT (left), single-PRT (middle) and dual-PRF (right) measurements.